Eur. Phys. J. Appl. Phys. (2015) 72: 31201
DOI: 10.1051/epjap/2015150301

THE EUROPEAN PHYSICAL JOURNAL APPLIED PHYSICS

Regular Article

Electronic, vibrational and thermodynamic properties of $Ca_{10}(AsO_4)_6(OH)_2$: first principles study

Yuanlei Zheng[1], Tao Gao[1,2,a], Yanrong Gong[1], Shenggui Ma[1], Mingli Yang [1,2], and Piheng Chen[3]

[1] Institute of Atomic and Molecular Physics, Sichuan University, 610065 Chengdu, P.R. China
[2] Key Laboratory of High Energy Density Physics and Technology of Ministry of Education, Sichuan University, 610064 Chengdu, P.R. China
[3] Science and Technology on Surface Physics and Chemistry Laboratory, 621907 Mianyang, P.R. China

Received: 11 June 2015 / Received in final form: 15 September 2015 / Accepted: 15 October 2015
Published online: 1 December 2015 –

Abstract. The electronic, vibrational and thermodynamic properties of johnbaumite (AHAP $Ca_{10}(AsO_4)_6(OH)_2$) have been performed by First principles approach. AHAP is an indirect band-gap material of 3.98 eV. The calculated phonon dispersion indicates that AHAP is stable. For AHAP, the optical vibrational modes at the Γ-point are assigned: 21E1 + 19A + 22E2 + 24B, and the frequencies agree well with available experimental data. The largest LO-TO phonon frequency splitting occurs at A mode (770.2 cm^{-1} to 807.6 cm^{-1}). Finally, the thermodynamic properties of AHAP are predicted.

1 Introduction

Johnbaumite (AHAP) is an arsenate analog of hydroxyapatite (HAP). Arsenic is well known for its acute toxicity. Thus chronically exposed to arsenic-contaminated water, arsenic will be absorbed into human body and deposited in bones. As a result, the arsenate may substitute for phosphate in HAP, the main inorganic component of bones. When the phosphorus in HAP is completely substituted by arsenic AHAP is formed [1,2].

Moreover, great attentions have been paid to AHAP in dealing with arsenic pollution problem, because arsenic removal from water and wastes would produce AHAP. For example, adding lime (CaO) into arsenic-containing waste would product precipitate-AHAP [3]. Using HAP to eliminate arsenic from water also produce AHAP due to the ionic-exchange between arsenic and phosphorus [4].

Consequently, there are a few relevant experimental studies on the crystal structure of AHAP. Lee et al. [5] examined arsenate (As^{5+}) substitution in HAP and reported the crystal structure of AHAP. Henderson et al. [6] studied the crystal structure of natural AHAP. The structural parameters that they obtained are in agreement with the work of Lee et al. Recently, Biagioni and Pasero [7] used the single-crystal X-ray diffraction to analyze the specimen of AHAP. Kusachi et al. [8] measured infrared absorption spectrums of mineral AHAP. In experiment, it is difficult to analyze multiphase infrared absorption spectrum, because the infrared spectrum of a single crystal is different from its powder [9].

There are many related experiment investigates the structural characterization of the AHAP, but theoretical calculation on the electronic, vibrational and thermodynamic properties of AHAP have not been found. In any case, proper interpretations of experimental data are based on the theoretical understanding on the material. It is well known that the thermodynamic properties, which play an important role on structural characterization of a material, are intimately relevant to the lattice dynamics. Moreover, phonon dispersion curves of a system without any imaginary frequencies indicate that the system is stable. Thus, calculation electronic, vibrational and thermodynamic properties of AHAP by density functional theory are meaningful. Taking into consideration that AHAP is isomorphous with HAP, we compared the electronic and vibrational properties of AHAP with that of HAP. For AHAP, we assigned the infrared and Raman active vibrational modes at the Γ-point. In experiment, the LO-TO phonon frequencies splitting cannot be observed. But through our calculation, the LO-TO phonon frequencies splitting of AHAP at the Γ-point were obtained. Finally, we predicted the thermodynamic properties for AHAP, such as Helmholtz free energy ΔF, internal energy ΔE, constant-volume specific heat C_v and entropy S.

2 Computational details

All the calculations were performed by the Vienna ab-initio simulation package (VASP) [10–14]. The dynamic properties have been calculated by the linear-response

[a] e-mail: gaotao@scu.edu.cn

approach based on the DFPT [15]. Atomic displacements are treated as perturbations, and the electronic response to the perturbation is calculated by self-consistent iteration. When the first-order responses have been obtained, the second derivatives of the total energy with respect to atomic displacements can be performed. The dynamical matrices can be further calculated by the Fourier transform. Pseudo-potentials were treated with the projected augmented wave method (PAW) [16]. The exchange correlation energy was described by the Perdew-Wang (PW91) [17] exchange-correlation functional with the generalized gradient approximate (GGA). We used 500 eV as the kinetic energy cutoff for bulk calculations. The optimized structure has been obtained after a full relaxation of the cell. A $3\times3\times4$ Gamma-centered k-point mesh for the Brillouin zone (BZ) was used. The convergence criterion for the total energy was 0.01 meV/cell.

3 Results and discussion

3.1 Structural analysis

AHAP is isomorphous with HAP. The crystal structure of HAP obtained by Kay et al. [18] and the structural view along the c-axis is shown in Figure 1. In comparison with HAP, the cell parameters and volume of AHAP are expansion, which is caused by larger size of AsO_4 tetrahedron than PO_4. While As substitute for P in HAP, the dilation lies is perpendicular to c axis. As a result, the cell parameter of AHAP expands along a direction and the cell parameters larger than HAP. The structural difference between AHAP and HAP also display in the twist angle of metaprism (Ca_1O_6) which is compose by Ca_1 atom with the nearest six O atoms. The twist angle of metaprism (Ca_1O_6) in AHAP is 23.5°, which is smaller than that in HAP [5], because the twist angle decreases with the increased size of the AsO_4 tetrahedron [19].

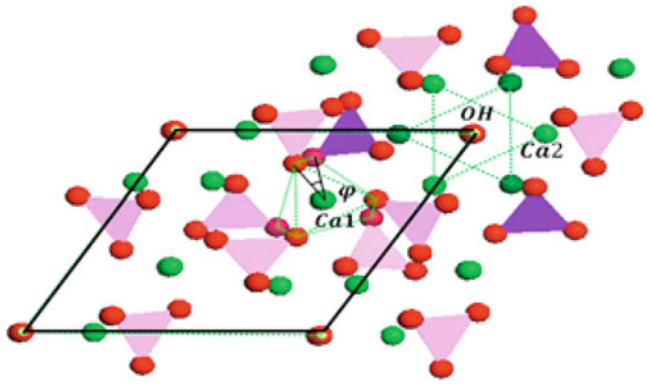

Fig. 1. View of HAP structure along the c axis. Six Ca2 atoms around the OH column form two triangular planes. The plans are drawn with green dotted lines. The metaprism formed by Ca1 atom and six O atoms also marked with green dotted lines. The twist angle φ of Ca_1O_6 metaprism is presented.

The experimental parameters of HAP are $a = b = 9.432$ Å, $c = 6.881$ Å, $\alpha = \beta = 90°$, $\gamma = 120°$ and volume is 530.14 Å^3 [18]. The cell parameters of synthetic AHAP are $a = b = 9.716$ Å, $c = 6.986$ Å, $\alpha = \beta = 90°$, $\gamma = 120°$ and volume is 571.06 Å^3 [5]. After electronic and ionic optimization, the structure of HAP relax to $a = b = 9.549$ Å, $c = 6.896$ Å, $\alpha = \beta = 90°$, $\gamma = 120°$ and volume is 544.58 Å^3, and AHAP relax to $a = b = 9.988$ Å, $c = 6.924$ Å, $\alpha = \beta = 90°$, $\gamma = 120°$ volume is 598.21 Å^3. Clearly, all the differences are in a reasonable error range. Compared to experimental results, our optimized structures of HAP and AHAP are reliable.

3.2 Band structure and density of states

The band structures for AHAP and HAP are shown in Figure 2. Both of them are indirect-gap materials. The band gap of AHAP is 3.95 eV and HAP is 5.25 eV which is in agreement with previously reported GGA band gap of 5.23 eV [20].

Figure 3 presents total DOS (TDOS) and PDOS of Ca atoms, tetrahedron and OH groups for AHAP and HAP. PDOS for each kind of atom are shown in Figure 4. In Figure 3, it is clearly shown that the top of valence band has three main peaks (A–C) within the energy range from −8 to 0 eV for AHAP. However, there are four main peaks (A–D) for HAP. These results are in agreement with the results reported by Rulis et al. [21]. These peaks are mostly dominated by the states of tetrahedron groups. For AHAP, peak A is determined by O_p and As_s states. Peak B is dominated by O_p and As_p states with tiny H_s contribution. Peak C is mostly from O_p contribution. For HAP, the peak A is mainly composed of O_p, O_s and P_s states. Peak B is dominated by O_p and P_p states. Peak C and peak D are dominated by O_p states. In the range of −16 to −20 eV, there are also two remarkable peaks, denoted by 1 and 2. For AHAP, the peak 1 is associated primarily with Ca_p states with some contribution from As_s and O_s states. Peak 2 is composed of O_s states. For HAP, peak 1 is mostly composed by Ca_p states. The peak 2 is dominated by O_s states. The conduction band of the two crystals, presented in Figure 3, is composed of unoccupied Ca states.

3.3 Vibrational properties

3.3.1 The phonon band structure and density of states

Based on the DFPT method [15], we calculated the vibrational properties of AHAP and HAP. In order to reach high precision, we used a $2\times1\times2$ supercell containing 176 atoms for the calculation. The phonon dispersion curves and density of phonon states of AHAP and HAP are shown in Figures 5 and 6. It has to notice that in one acoustic mode there are slight imaginary frequencies along Γ-A for both of AHAP and HAP. The largest value of imaginary frequency of HAP is about −0.18 THz (−6 cm^{-1}) and that of AHAP is about

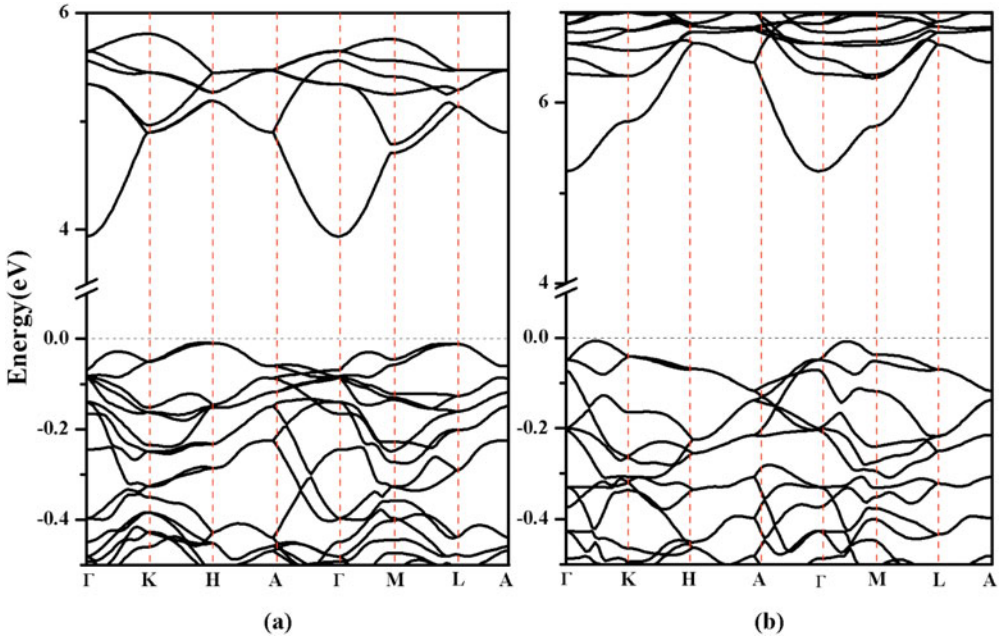

Fig. 2. Calculated band structures for AHAP (a) and HAP (b).

−0.15 THz (−5 cm^{-1}). Although there are slight imaginary frequencies in one acoustic mode, it doesn't indicate that our systems are unstable. This tiny imaginary frequency might be caused by the complication of AHAP and HAP systems. There are 176 atoms in calculation of vibrational properties, so it is highly time-consuming and hardware-consuming to adjust every atom accurate located in their balance positions. Actually in the related literature that computed the phonon frequencies of hydroxyapatite, we also found there are slight imaginary frequencies along Γ-A [22]. Furthermore, we find in other literatures that a stable system also exist slight imaginary near the Γ-point [23,24]. Thus, we think our computed results reliable, and the phonon dispersion curves

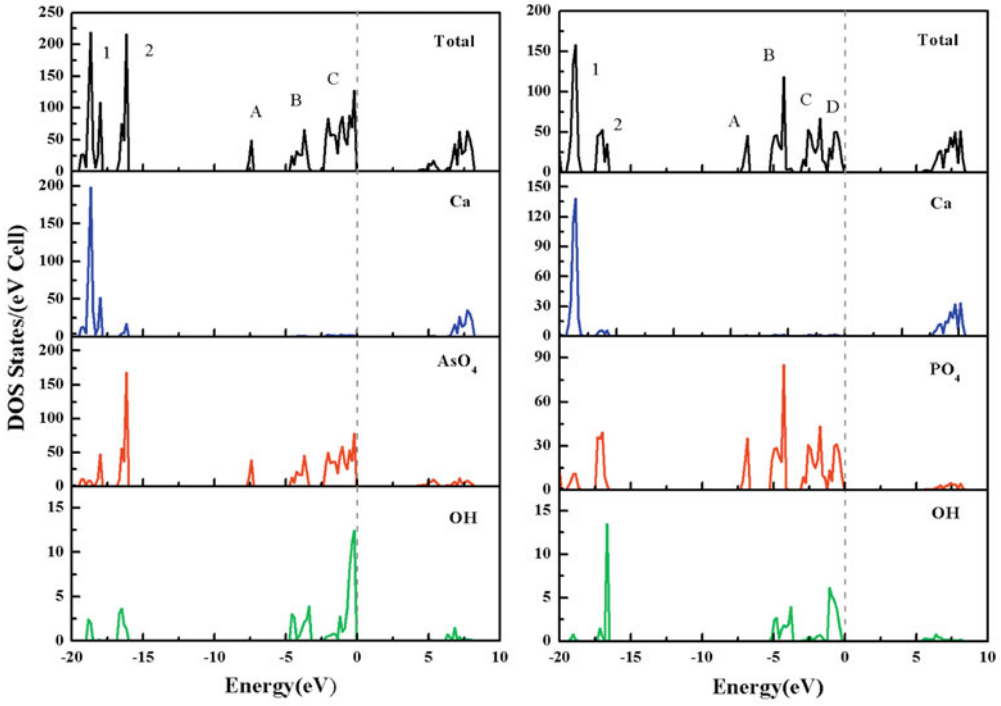

Fig. 3. Total density of states (TDOS) and combined partial density of states (PDOS) for AHAP and HAP.

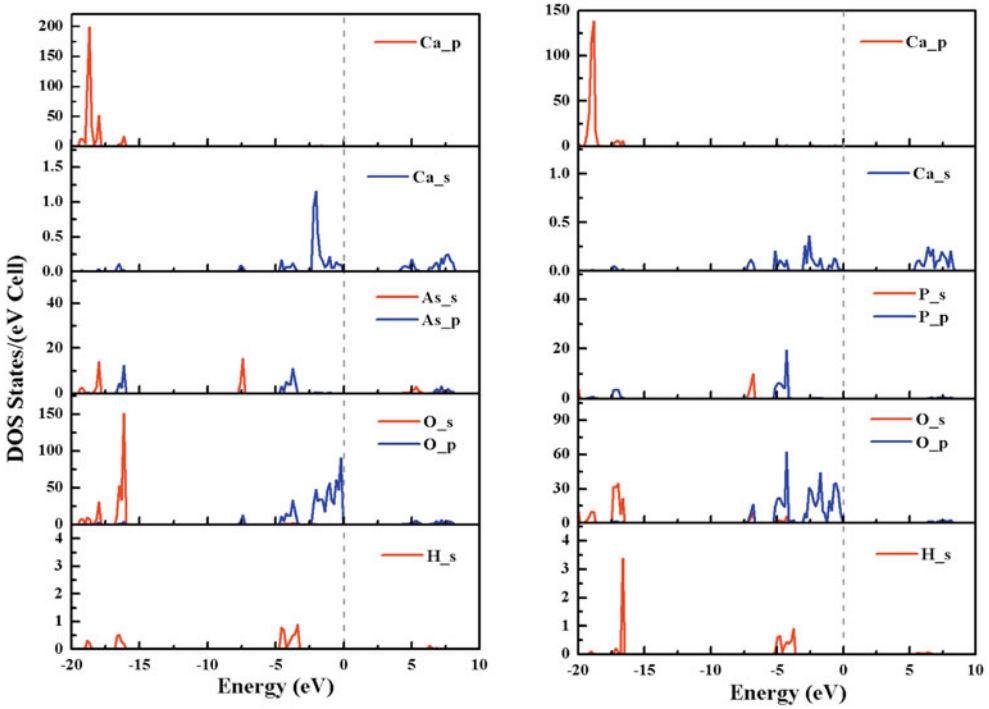

Fig. 4. PDOS of each kind of atoms for AHAP and HAP.

of AHAP and HAP still indicate that the two systems are stable. For AHAP, the bands below 292 cm^{-1} involve Ca atoms and AsO_4 group vibrations. The modes ranging from 311 to 480 cm^{-1} and from 744 to 913 cm^{-1} are mainly the AsO_4 vibrations. The modes at 669 and 3627 cm^{-1} is corresponding to the libration and stretching vibration of OH. The characteristic of AsO_4 is around 440 and 880 cm^{-1}, and the stretching vibration of OH group is 3500 cm^{-1}. This result is in agreement with the experimental result [8]. For HAP, the modes in the range of 382–610 cm^{-1} and 894–1083 cm^{-1} are the PO_4 vibrations. The libration and stretching modes of OH are 667 and 3640 cm^{-1} respectively, and the calculated frequencies agree with other theoretical predictions too [22]. Compared with HAP, the stretching vibrational frequency of OH in AHAP is smaller. We think this result comes from As atoms effects. This calculated result consists with the experimental results [5].

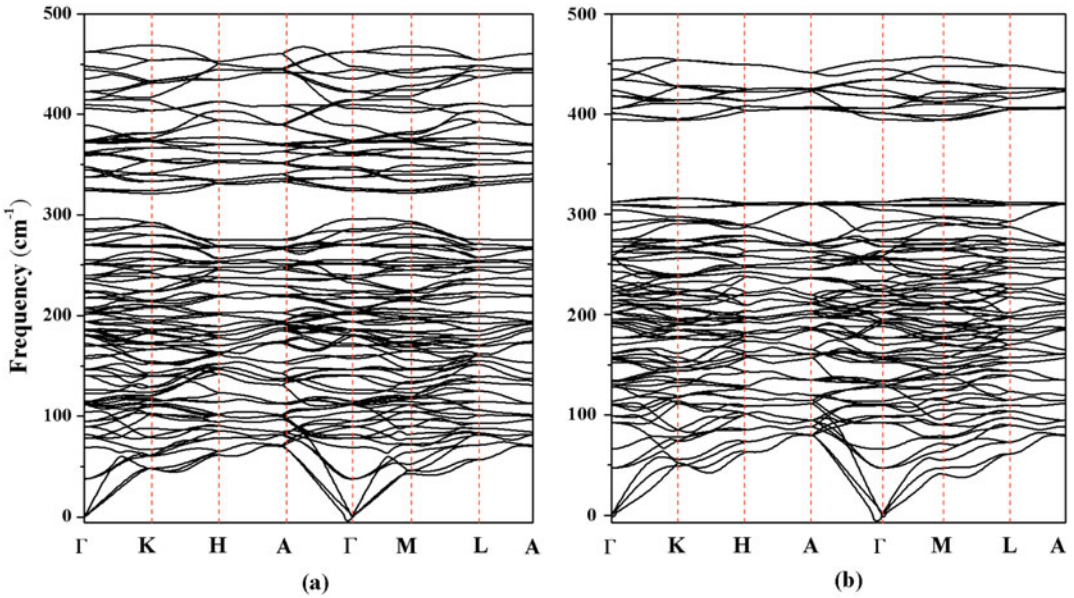

Fig. 5. Phonon dispersion curves for AHAP (a) and HAP (b).

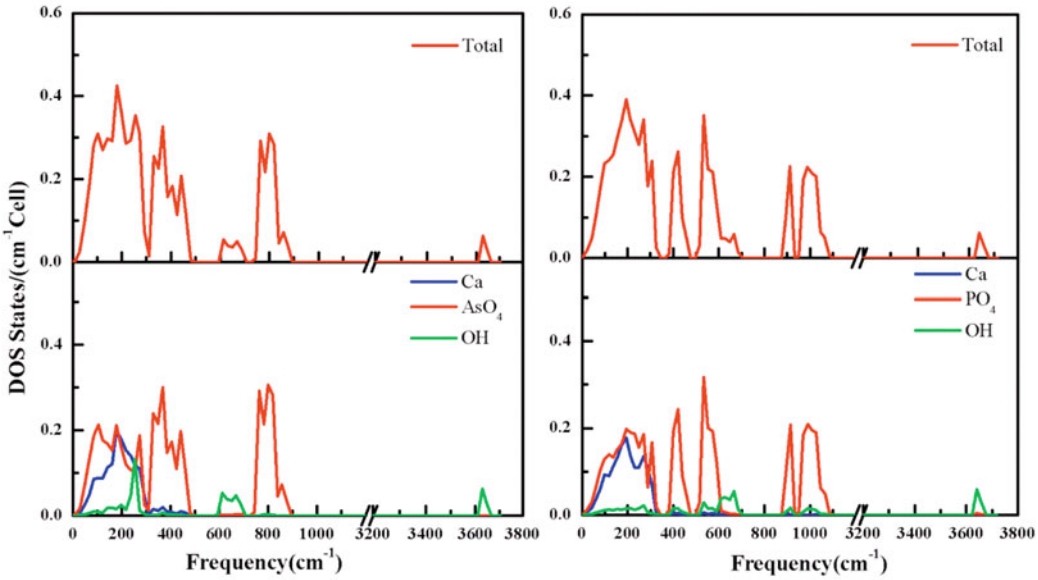

Fig. 6. Density of phonon states for AHAP and HAP.

3.3.2 The LO-TO splitting

For insulators, taking dipole-dipole (long-range Coulomb) interaction into consideration can obtain a split between longitudinal (LO) and transverse (TO) optical phonon frequencies at the Γ-point [25]. The phonon frequencies and the assignment of infrared- and Raman-active optical modes, as well as the LO-TO splitting at the Γ-point are provided in Table 1. There are 44 atoms in AHAP unit cell with 129 optical and 3 acoustic vibrational modes among the 132 vibrational modes. AHAP belong to point group C6. The character table indicates that there are four irreducible representations. Symmetry decomposition of optical vibrational modes according to a standard group-theoretical analysis at the Γ-point is as follows: 21E1 + 19A + 22E2 + 24B. A and E1 modes are both infrared

Table 1. Calculated phonon frequencies (in cm^{-1}) and the assignment of the infrared- and Raman-active optical modes, LO-TO splitting at Γ-point.

IR		Raman		
E1(LO/TO)	A(LO/TO)(**exp***)	E1	A	E2
38.1/37.9	104.5/104.4	37.9	104.4	89.6
85.0/78.2	114.0/112.9	78.2	112.9	95.0
112.1/111.7	158.3/157.5	111.7	157.5	111.5
152.3/146.5	180.5/180.4	146.5	180.4	114.9
170.3/170.1	194.1/194.0	170.1	194.0	140.6
203.6/186.4	202.1/202.0	186.4	202.0	180.1
204.6/203.9	223.6/222.1	203.9	222.1	185.0
220.7/207.4	257.7/232.2	207.4	232.2	194.1
240.0/236.3	276.0/275.1	236.3	275.1	217.4
269.6/250.9	292.0/283.5	250.9	283.5	239.3
305.2/270.5	348.5/347.8	270.5	347.8	251.6
326.4/326.3	376.3/360.5	326.3	360.5	269.7
367.1/362.2	405.9/389.1	362.2	389.1	337.3
380.2/373.5	435.5/406.1	373.5	406.1	345.0
414.4/414.2	457.4/435.6(**440**)	414.2	435.6	371.8
459.3/422.9	764.1/764.0	422.9	764.0	374.2
620.6/610.0	807.6/770.2	610.0	770.2	462.4
774.3/774.2	838.7/807.7	774.2	807.7	682.6
792.6/778.5	3634.1/3633.7	778.5	3633.7(**3500**)	760.7
817.1/806.0		806.0		787.6
863.9/828.6(**880**)		828.6		806.1
				820.8

*Reference [8].

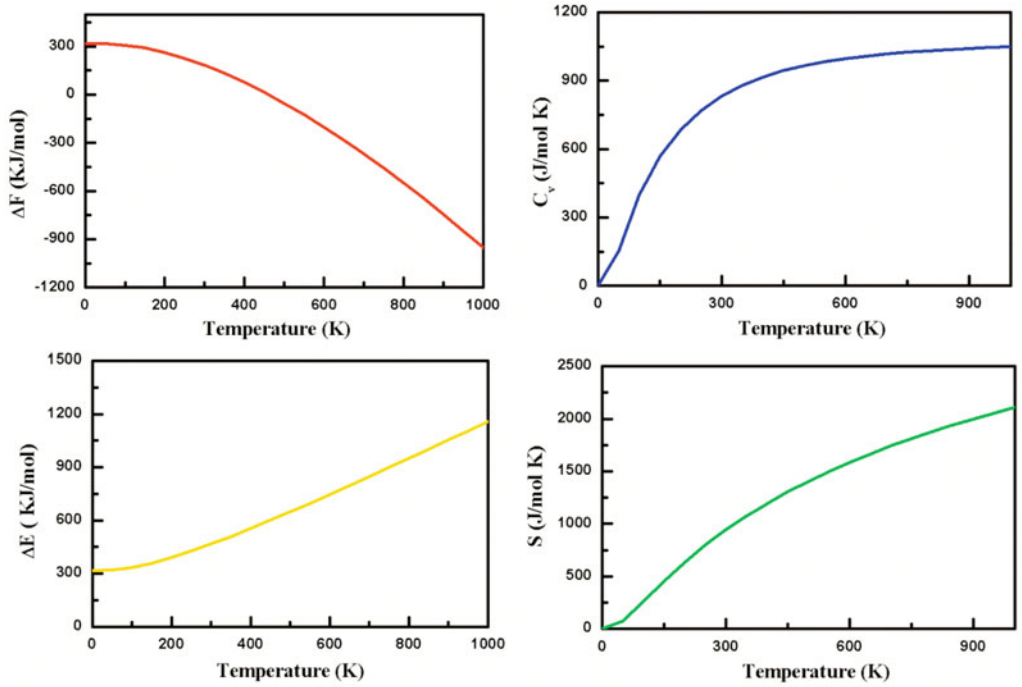

Fig. 7. The phonon contributions to Helmholtz free energy ΔF, internal energy ΔE, constant-volume specific heat $C_{\rm v}$ and entropy S as a function of temperature for AHAP.

and Raman active modes. E2 modes are only Raman active without LO-TO splitting and B modes are silent modes. The largest frequency difference of LO-TO splitting is about 37 $\rm cm^{-1}$ occurring in A mode (770.2 $\rm cm^{-1}$ to 807.6 $\rm cm^{-1}$).

3.4 Thermodynamic properties

The thermodynamic properties have been obtained from the density of phonon states by harmonic approximation [26]. It has been confirmed that the stoichiometric apatites decompose at about 1200 °C (1475 K) [27]. The X-ray patterns of AHAP in the range of 383–1073 K indicate that there is no phase transitions occur in this temperature range [28]. Therefore, the thermodynamic functions for AHAP such as the Helmholtz free energy ΔF, internal energy ΔE, constant-volume specific heat $C_{\rm v}$, and entropy S have been calculated, and the results are presented in Figure 7. We have calculated ΔF_0 and ΔE_0 at zero temperature, and the values are both 317.6 kJ/mol. The functional values of ΔF, ΔE, $C_{\rm v}$ and

Table 2. Thermodynamic functions for AHAP.

T (K)	ΔF (kJ/mol)	S (J/mol K)	$C_{\rm v}$ (J/mol K)	ΔE (kJ/mol)
250	227.3	797.6	769.3	426.7
300	183.7	943.7	832.2	466.8
350	133.2	1075.7	879.7	509.7
400	76.3	1195.7	915.9	554.6
450	13.8	1305.2	943.8	601.1
500	−54.0	1405.8	965.6	648.9
550	−126.7	1498.7	982.9	697.6
600	−203.8	1584.8	996.8	747.1
650	−285.1	1665.1	1008.1	797.2
700	−370.2	1740.1	1017.4	847.9
750	−459.0	1810.6	1025.2	899.0
800	−551.2	1877.0	1031.9	950.4
850	−646.6	1939.7	1037.5	1002.1
900	−745.1	1999.2	1042.4	1054.1
950	−846.5	2055.7	1046.7	1106.4
1000	−950.6	2109.4	1050.5	1158.8

S in the range of 250–1000 K are given in Table 2. At high temperature, C_v reaches a classic limit of 1097 J/K mol which is in good agreement with the classic equipartition law.

4 Conclusions

We have performed first-principles calculations of the electronic structure, vibrational and thermodynamic properties of AHAP. The band gap of AHAP is 3.95 eV and HAP is 5.25 eV. Compared with HAP, we find that AHAP display similar electronic properties.

Based on DFPT, the vibrational properties of AHAP and HAP have been determined. The calculated frequencies are in good agreement with experimental results. Compared with HAP, the stretching vibrational frequency of OH in AHAP is smaller. The infrared and Raman active modes at the Γ-point for AHAP were assigned. The largest difference between LO and TO frequency is 37 cm^{-1} (770.2–807.6 cm^{-1}), occurring in A modes.

The thermodynamic functions of AHAP such as ΔF, ΔE, C_v and S have been calculated by harmonic approximation. We calculated ΔF_0 and ΔE_0 at zero temperature, and the values are both 317.6 kJ/mol. We hope that these results will provide a useful guidance for structural characterization of AHAP.

This work was financially supported by the National High Technology Research and Development Program of China (2015AA034202) and the National Natural Science Foundation of China (No. 11305147).

References

1. J.T. Hindmarsh, R.F. McCurdy, J. Savory, Crit. Rev. Clin. Lab. Sci. **23**, 315 (1986)
2. World Health Organization, Geneva, 2001
3. J.V. Bothe, P.W. Brown, Environ. Sci. Technol. **33**, 3806 (1999)
4. A.E. Wendlandt, W. Harrison, R. Wendlandt, *Geological Society of America Annual Meeting, Denver, Colorado, USA, 2002*. Available from `http://gsaconflexcom/gsa/2002AM/finalprogram/abstract_44300htm`
5. Y.J. Lee, P.W. Stephens, Y. Tang, W. Li, B.L. Phillips, J.B. Parise, R.J. Reeder, Am. Mineral. **94**, 666 (2009)
6. C. Henderson, A. Bell, J. Charnock, K. Knight, R. Wendlandt, D. Plant, W. Harrison, Mineral. Mag. **73**, 433 (2009)
7. C. Biagioni, M. Pasero, Am. Mineral. **98**, 1580 (2013)
8. I. Kusachi, C. Henmi, S. Kobayashi, Mineral. J. **18**, 60 (1996)
9. L. Calderin, D. Dunfield, M. Stott, Phys. Rev. B **72**, 224304 (2005)
10. G. Kresse, J. Hafner, Phys. Rev. B **47**, 558 (1993)
11. G. Kresse, J. Hafner, J. Phys.: Condens. Matter **6**, 8245 (1994)
12. G. Kresse, J. Furthmüller, Phys. Rev. B **54**, 11169 (1996)
13. G. Kresse, D. Joubert, Phys. Rev. B **59**, 1758 (1999)
14. G. Kresse, J. Furthmüller, Comput. Mater. Sci. **6**, 15 (1996)
15. X. Gonze, C. Lee, Phys. Rev. B **55**, 10355 (1997)
16. P.E. Blöchl, Phys. Rev. B **50**, 17953 (1994)
17. J.W. Yang, T. Gao, L.Y. Guo, Physica B: Condens. Matter **429**, 119 (2013)
18. M. Kay, R. Young, A. Posner, Nature **204**, 1050 (1964)
19. T.J. White, Z. Dong, Acta Crystallogr. B: Struct. Sci. **59**, 1 (2003)
20. A. Slepko, A.A. Demkov, Phys. Rev. B **84**, 134108 (2011)
21. P. Rulis, L. Ouyang, W. Ching, Phys. Rev. B **70**, 155104 (2004)
22. S.S. Bhat, U.V. Waghmare, U. Ramamurty, Cryst. Growth Des. **14**, 3131 (2014)
23. L. Zhu, L. Li, T.-M. Cheng, Comput. Mater. Sci. **106**, 135 (2015)
24. L. Zhu, L. Li, T. Cheng, D. Xu, J. Mater. Chem. A **3**, 5449 (2015)
25. X. Gonze, J.-C. Charlier, D. Allan, M. Teter, Phys. Rev. B **50**, 13035 (1994)
26. C. Lee X. Gonze, Phys. Rev. B **51**, 8610 (1995)
27. P. Mahapatra, L. Mahapatra, B. Mishra, Bull. Chem. Soc. Jpn **62**, 3272 (1989)
28. P. Mahapatra, L. Mahapatra, B. Mishra, Polyhedron **6**, 1049 (1987)